Bidirectional Harmonic Current Control of Brushless Doubly Fed Motor Drive System Based on a Fractional Unidirectional Converter Under a Weak Grid

ZHENPING LI[1], **XUEFAN WANG**[1], **MING KONG**[1,2], **AND XI CHEN**[1], **(Member, IEEE)**

[1]State Key Laboratory of Advanced Electromagnetic Engineering and Technology, Huazhong University of Science and Technology, Wuhan 430074, China
[2]EAST Group Company Ltd., Dongguan 523808, China

Corresponding author: Xi Chen (eechenxi@gmail.com)

ABSTRACT The brushless doubly fed machine (BDFM) drive system based on a fractional unidirectional converter is a promising low-cost variable-speed drive system, which shows great potential in applications of driving fans and pumps. However, the harmonic current generated by a diode rectifier can flow into the machine and the grid under a weak grid, which will cause a 6th-order frequency torque ripple and lead to voltage distortion. A steady equivalent circuit considering the uncontrolled rectifier and the grid impedance is built firstly to study the harmonic distribution characteristics. To eliminate the influence of harmonic currents, the harmonic equivalent impedance of the machine system should be regulated to change the harmonic distribution characteristics. This paper improves the conventional control method through adding a harmonic control loop to prevent harmonic currents from being injected into the machine or the grid, which is then applied in the fundamental synchronous frame. Two indirect parameters are selected to realize the two control targets. Afterwards, the influence of the control system on the harmonic equivalent impedance of the machine system under the conventional method and the proposed method are compared. Finally, experimental results obtained from a 30 kW BDFM prototype verify the proposed method.

INDEX TERMS Brushless doubly fed machine, fractional unidirectional converter, harmonic current control, weak grid.

I. INTRODUCTION

The continued development of brushless doubly fed machines (BDFMs) has led to increasingly mature design and control methods [1], [2]. As a highly reliability machine, BDFM offers the advantages of fractional rated power converter requirements and indirect control characteristics, making it a preferred device in specific fields. When working as a generator, BDFM can be applied to standalone generation [2], hydropower generation [3] and wind power generation [4]. In addition, its superiority in the field of variable speed drive systems, especially high-voltage drive systems is also significant.

Similar to doubly fed induction machine (DFIM), BDFM has two sets of stator windings: one set, the power winding (PW), is connected to the grid directly, while the other set, the control winding (CW), is controlled by the converter. As a multi-port electrical machine, the operation state of the BDFM is determined by the excitation sources on two stator windings and the load on the shaft. The electromotive force of the PW and electromagnetic torque can be regulated by changing the output voltage amplitude, phase and frequency of the converter.

At the super-synchronous speeds, the power of the two stator windings flows from the power supply to the motor. Some fan and pump loads generally only need limited range speed regulation. Thus, the BDFM controlled by a fractional unidirectional converter is a reliable scheme for these applications. A chopper circuit could be applied to realize the
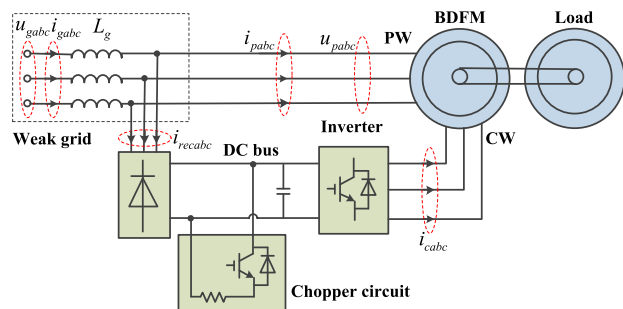
The associate editor coordinating the review of this manuscript and approving it for publication was Mohsin Jamil.

Z. Li *et al.*: Bidirectional Harmonic Current Control of BDFM Drive System Based on a Fractional Unidirectional Converter

IEEE Access

FIGURE 1. The structure of the BDFM drive system with a unidirectional converter.

starting process [5]. However, a number of harmonic currents would be injected into the power system. Moreover, the PW voltage could deteriorate under a weak grid. The structure of the BDFM drive system based on a unidirectional converter is shown in Fig. 1. The grid resistance is far less than the harmonic reactance that can be ignored, while L_g represents the grid equivalent inductance in Fig. 1.

Most control methods for BDFM assume that the system operates under a normal [6], [7] or unbalanced grid [8], [9]. In [6], the unidirectional converter was applied and a simple closed-loop scalar control strategy was introduced based on the torque-angle characteristic. A sliding-mode control method was presented in [7] to obtain quick dynamic responses. Unbalanced grid conditions were generally considered in wind power generation [8] and stand-alone power systems [9]. Although the reasons making the grid unbalanced are different, the control strategies of the two conditions were similar. With an increasing proportion of nonlinear loads, especially from the broad use of unidirectional converters, terminally weak grids can create harmonic distortion. Control methods for DFIM generation systems working under distorted grids were widely studied in [10]–[13]. A sensorless control method for the standalone BDFM generator with unbalanced and nonlinear loads was applied in [14]. In [10]–[12], as a part of the grid, the capacity of doubly-fed generator is far less than the distorted grid. The harmonic distortion of the grid voltage is assumed constant. To improve the generator operation is the major control objectives, such as elimination of the stator harmonic currents [10], [11], reduction of the active and reactive power oscillation [12]. In the power grids introduced in [13] and [14], the DFIM and BDFM are the unique independent power supply for the system. Due to the existence of unbalanced and nonlinear loads, the voltage at the point of common coupling (PCC) is distorted. The influence is eliminated by controlling the output of the generator and the line side part of the back-to-back converter.

When BDFM works as a motor, the converter using a diode rectifier can obviously reduce the system cost. In this operating state, the harmonic currents of the rectifier increase with the increasing converter output power. In a weak grid, the PCC voltage would result in a distortion which would be varied with the increasing harmonic current and may degrade

the operational environment of other devices. The limitations of power system maximum distortion were outlined in [15]. However, the harmonics distribution characteristics in this system and the control targets are different with the power generation system in [10]–[14]. The harmonic distortion of the grid voltage is not constant. Moreover, both the uncontrolled rectifier and the BDFM are the loads of the power grid. Thus, it is necessary to study the effects of this kind of drive system and regulate the harmonic currents effectively.

This paper proposes a harmonic current control method to eliminate harmonic influence on the machine or the grid for this BDFM driving system. The resonance controller is applied to implement the harmonic control loop which can reduce the calculation time of coordinate transform. Main contributions of this paper are:

1) Proposing a complete circuit model of the BDFM drive system by including unidirectional converter and grid impedance to analyze harmonic distribution characteristics;

2) Improving the control method to regulate the system harmonic distribution characteristic through changing the machine harmonic equivalent impedance by selecting the PW current and voltage as the effective control parameters.

In section II, the frequency and power characteristics of BDFM are introduced. The uncontrolled rectifier is equated to a harmonic current source that is applied to the BDFM steady equivalent circuit. Then, the harmonic current distribution characteristics of the BDFM drive system under a weak grid and different load conditions can be obtained. Two control targets, which are reducing the harmonic currents flowing into the BDFM and improving the PCC voltage, are separately defined in section III. Moreover, the transfer functions corresponding to the targets in the conventional control method are derived. The harmonic frequency response characteristics are also studied. In section IV, harmonic control loops are added to optimize the system, and the transfer functions in the proposed control structure are presented. In section V, the proposed control methods are realized and verified in a 30 kW BDFM drive system. Finally, the conclusion of this study is presented in section VI.

II. HARMONIC DISTRIBUTION CHARACTERISTICS OF THE BDFM SYSTEM

Some distributed loads in remote regions, such as pumping units, connect to the grid through individual small-capacity transformers. Since the PCC voltage would be affected by the load currents, the grid impedance in this condition cannot be neglected if compared with the ideal grid. Therefore, it can be regarded as a weak grid. The analysis of grid impedance in this paper represents the impact of the weak grid.

According to the equivalent circuit of the BDFM, it is positive correlation between the active power and frequency of the two stators [16]:

$$P_p/P_c = f_p/f_c \qquad (1)$$

where P represents the active power flowing into the machine, f is the frequency of the excitation source, and the

IEEE *Access*

Z. Li *et al.*: Bidirectional Harmonic Current Control of BDFM Drive System Based on a Fractional Unidirectional Converter
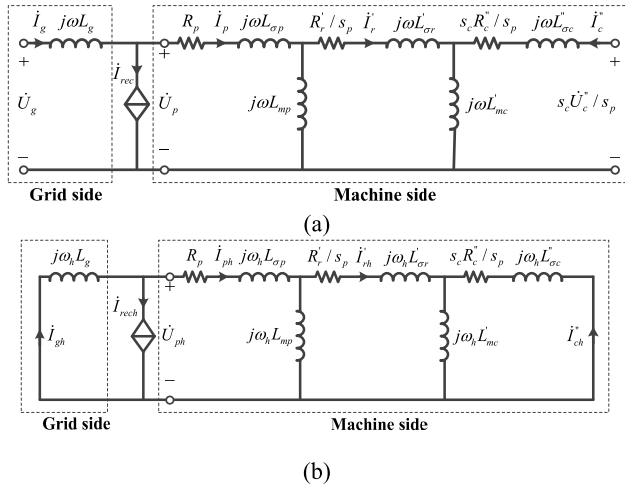

FIGURE 2. The equivalent circuit considering the unidirectional converter and grid impedance: (a) The generalized equivalent circuit of BDFM system; (b) The equivalent circuit of harmonic components.

subscripts "p" and "c" represent the PW side and CW side, respectively.

In cascading mode, the converter output frequency should satisfy (2) for steady operation according to [17].

$$f_c = \frac{(p_p + p_c)n_r}{60} - f_p \qquad (2)$$

where p is the pole pairs of the stator winding and n_r represents the machine speed.

Generally, f_p is equated to a constant number (the grid frequency) for the direct connection between the PW and the grid. According to (1) and (2), the active power ratio of the CW is positively correlated with the motor speed if above the natural synchronization speed. The harmonic currents generated by the uncontrolled rectifier increase with its increasing power output. If the grid impedance cannot be ignored, the harmonic current would be injected into the grid and machine. In [18], the steady equivalent circuit for BDFM was presented. If considering the power grid impedance and diode rectifier, a new equivalent circuit could be obtained, which is shown in Fig. 2(a).

The controlled current source $\dot{I}_{rec}$ represents the rectifier, ω represents the circuit angular frequency, L_σ represents the leakage inductance, L_m represents the magnetizing inductance between the stator and rotor, R represents the resistor of the stator and rotor windings, s_p and s_c are the slip of the PW side and CW side, respectively.

According to [19], the magnetic field of BDFM is established by the PW side and CW side together. Since the PW connects directly to the grid, the power factor of the PW can be maintained within a certain range. A proper setting of the PW and CW excitation current can prevent the stator and rotor iron from being saturated. The harmonic equivalent circuit shown in Fig. 2(b) can be separated from Fig. 2(a) based on the superposition theorem when the machine operates in ideal conditions, namely, the iron is not saturated. Considering $\dot{U}_c$

as a pure sinusoidal source, the CW side can be equated to the short circuit in Fig. 2(b).

It is obvious that $\dot{I}_{ph}$ would be close to zero in Fig. 2(b) if Z_{gh} $(j\omega_h L_g)$ is far less than the BDFM equivalent impedance. The harmonic currents of nonlinear loads would have little effect on the machine. In contrast, if the impedance of the power grid and BDFM are in the same order, a part of $\dot{I}_{rech}$ would flow into the machine. Moreover, the harmonic voltage dip on L_g would also distort $\dot{U}_p$ in Fig. 2(b). In this case, the power system can be seen as a weak grid.

Through the circuit shown in Fig. 2(b), the source of $\dot{I}_{ph}$ is the nonlinear load in the local power system. In this harmonic circuit, the machine side part could be equated to a Z_M. It can be derived as:

$$Z_M = \frac{j\omega_h L_{mp}(s_c R_r' R_c'' - \omega_h^2 a_1) - \omega_h^2 L_{mp} a_2}{j\omega_h a_3 + s_c R_r' R_c'' - \omega_h^2 a_4} + R_p + j\omega_h L_{\sigma p} \qquad (3)$$

where $a_1 a_2$, a_3, and a_4 are expressed as

$$a_1 = s_p^2(L_{\sigma r}' L_{\sigma c}'' + L_{\sigma c}'' L_{mc}' + L_{\sigma r}' L_{mc}')$$
$$a_2 = s_p(s_c R_c'' L_{mc}' + s_c R_c'' L_{\sigma r}' + R_r' L_{mc}' + R_r' L_{\sigma c}'')$$
$$a_3 = s_p(s_c R_c'' L_{mp} + s_c R_c'' L_{mc}' + s_c R_c'' L_{\sigma r}' + R_r' L_{mc}' + R_r' L_{\sigma c}'')$$
$$a_4 = s_p^2(L_{\sigma r}' L_{\sigma c}'' + L_{\sigma c}'' L_{mc}' + L_{\sigma r}' L_{mc}' + L_{\sigma c}'' L_{mp} + L_{mc}' L_{mp}).$$

Assuming that the machine operates at a constant speed n_r, Z_M can be identified in the corresponding harmonic circuits. $\dot{I}_{rech}$ changes along with the converter output power. Thus, for a certain operational state, steady speed and load, $\dot{I}_{gh}$ and $\dot{I}_{ph}$ can be calculated. The harmonic current contents in the machine and the grid are determined by the grid harmonic impedance and the harmonic equivalent impedance of the machine system.

The harmonic components with different orders generated by the diode rectifier may inject into the grid or machine and their effects would be superimposed with each other. The higher order harmonics produced by diode rectifier load, such as 11th, 13th, and 17th, are so small that can be neglected. Thus, this paper only considers the major 5th and 7th components which are the major parts relative to other harmonic components [13]. Thus, $\dot{I}_{rech}$ can be expressed as:

$$\dot{I}_{rech} = \sqrt{2}I_{rec5}\cos(5\omega_g t + \varphi_5) + \sqrt{2}I_{rec7}\cos(7\omega_g t + \varphi_7) \qquad (4)$$

where the subscripts "5" and "7" represent the order of harmonic currents, ω_g is the grid frequency, φ is the initial phase angle, and the subscript "h" represents the harmonic components.

A 30 kW wound rotor BDFM prototype is applied to verify the analysis. The parameters of the equivalent circuit in Fig. 2(a) are shown in Table 1. The weak grid is built through a 1.2 mH 3-phase inductor series with the network. Then, the system is controlled and operated in asynchronous and cascade modes with different loads.

In the asynchronous mode, the CW is shorted directly. Thus, the effects of control loops can be shielded. On the

Z. Li et al.: Bidirectional Harmonic Current Control of BDFM Drive System Based on a Fractional Unidirectional Converter

IEEE Access

TABLE 1. Specifications of the 30 kW BDFM prototype.

Parameter	Value	Parameter	Value
R_p	0.1707 Ω	PW/CW pole pairs	1/3
$L_{\sigma p}$	0.0021 H	PW rated voltage	400 V
L_{mp}	0.2257 H	PW rated current	40 A
R_c''	0.2294 Ω	CW rated current	35 A
$L_{\sigma c}''$	0.0013 H	CW rated voltage	400 V
L_{mc}''	0.0647 H	rated power	30 kW
R_r'	0.3196 Ω	rated speed	1250 rpm
$L_{\sigma r}'$	0.0035 H	rotor type	wound

FIGURE 3. The calculation and measurement results of the 5th and 7th harmonic currents in the grid and machine side: (a) The asynchronous mode; (b) The cascade mode.

TABLE 2. The harmonic angular frequency of the machine.

	Fundamental	5th	7th
PW side	ω_p	$-5\omega_p$	$7\omega_p$
CW side	ω_c	$6\omega_p+\omega_c$	$-6\omega_p+\omega_c$
Rotor side	ω_{rs}	$-6\omega_p+\omega_{rs}$	$6\omega_p+\omega_{rs}$

in the analysis for small values. This effect may cause a variation in the machine equivalent harmonic impedance. For this reason, there is little difference between the measurement and calculation data shown in Fig. 3(b).

Through the harmonic circuit shown in Fig. 2(b), a steady harmonic torque can be calculated. This torque can be ignored for the small value of harmonic currents. In a weak grid, the harmonic currents flowing into BDFM can produce an alternative torque through the interaction of fundamental and harmonic magnetic fields. The value of the fundamental component is large enough relative to the harmonic components that the torque ripple cannot be ignored. As a multi-input machine, the induction potential of the PW can be regulated by controlling the converter which is connected to the CW. As the equivalent circuit is only suitable for steady characteristics analysis, a transient model is introduced to implement the harmonic current regulator under different control targets.

According to [20], the dynamic model of BDFM in unified reference frame is presented in (5):

$$\begin{cases} \boldsymbol{u}_p = R_p\boldsymbol{i}_p + s\boldsymbol{\psi}_p + j\delta_p\boldsymbol{\psi}_p \\ \boldsymbol{\psi}_p = L_{sp}\boldsymbol{i}_p + M_{pr}\boldsymbol{i}_r \\ \boldsymbol{u}_c = R_c\boldsymbol{i}_c + s\boldsymbol{\psi}_c + j\delta_c\boldsymbol{\psi}_c \\ \boldsymbol{\psi}_c = L_{sc}\boldsymbol{i}_c + M_{cr}\boldsymbol{i}_r \\ \boldsymbol{u}_r = R_r\boldsymbol{i}_r + s\boldsymbol{\psi}_r + j\delta_r\boldsymbol{\psi}_r \\ \boldsymbol{\psi}_r = M_{pr}\boldsymbol{i}_p + M_{cr}\boldsymbol{i}_c + L_{sr}\boldsymbol{i}_r \end{cases} \quad (5)$$

where Ψ, $\boldsymbol{u}$ and $\boldsymbol{i}$ represent the flux, voltage and current vector, "s" is the differential operator, δ is the angular frequency of the vectors, L_{sp}, L_{sc} and L_{sr} are the self-inductances of the PW, CW and rotor winding, M_{pr} and M_{cr} are the mutual-inductances between the stators (PW and CW) and the rotor, and subscripts "p", "c" and "r" represent the vectors of the three windings.

The relationships among δ_p, δ_c and δ_r can be expressed as:

$$\begin{cases} \delta_p = \omega_p t \\ \delta_r = \delta_p - p_p\omega_r \\ \delta_c = (p_p + p_c)\omega_r - \delta_p. \end{cases} \quad (6)$$

Assume that the fundamental angular frequencies of the PW, CW and rotor side are ω_p, ω_c and ω_{rs}, respectively. The harmonic frequency corresponding relations in Table 2 could be obtained directly according to (2). The calculation is based on the principle that the magnetic fields of the stator and rotor with the same number of pole pairs have the same rotational speed.

The vectors in the rotating reference frame could also be divided into the fundamental part, the negative sequence 5th
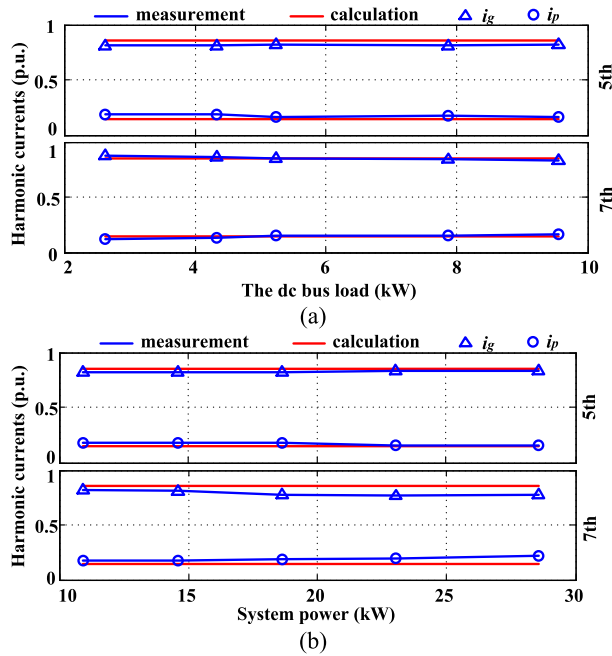
other hand, the power consumed by the converter is nearly zero. In order to obtain a sufficient value of $\dot{I}_{rech}$ for calculation, a resistance load is connected to the converter DC bus. In this way, $\dot{I}_{rech}$ can be changed by following the variation of resistance.

According to Fig. 2(b), the harmonic currents flowing into the grid and machine will also be changed. The measurement and calculation results of $\dot{I}_{ph}$ and $\dot{I}_{gh}$ based on different resistance loads are shown in Fig. 3(a). Z_m is only related to the machine speed and frequency of the harmonic current. In Fig. 3(a), the amplitudes of $\dot{I}_{ph}$ and $\dot{I}_{gh}$ are transformed into per-unit values using the amplitude of $\dot{I}_{rech}$ as the basic value. The amplitude curves of $\dot{I}_{ph}$ and $\dot{I}_{gh}$ are approximately linear for the constant proportion relationship. The measurement values are in consistent with the calculation results according to Fig. 2(b).

The measurement results of the cascade mode (1100 rpm) are shown in Fig. 3(b). Similar to the asynchronous mode, the proportions of $\dot{I}_{ph}$ and $\dot{I}_{gh}$ are approximately constant. In this mode, the converter is working for a stable system. The responses of control loops on harmonic currents are ignored

IEEEAccess

Z. Li *et al.*: Bidirectional Harmonic Current Control of BDFM Drive System Based on a Fractional Unidirectional Converter

part and the positive sequence 7th part as shown in (7):

$$\lambda = \lambda_1^1 + \lambda_5^5 e^{-j(6\omega_p t + \theta_5)} + \lambda_7^7 e^{j(6\omega_p t + \theta_7)} \qquad (7)$$

where λ represents the vector of flux, voltage and current; θ is the initial rotating angle of the reference frame, superscripts "1", "5" and "7" represent the fundamental, 5th and 7th components; subscripts "1", "5" and "7" represent the fundamental, 5th and 7th synchronous frames, respectively.

III. CONTROL TARGETS CONFIRMATION

In a drive system, the low THD (total harmonic distortion) of i_g and small torque ripple appear to be two important evaluation indexes. Considering that the grid currents need additional sensors and machine torque cannot be measured directly, the related replacements should be selected for control system design.

A. MACHINE TORQUE RIPPLE

As the diode rectifier connects with PW directly, partial harmonic currents of the converter are injected into the machine. The interaction of fundamental and harmonic components generates high-frequency torque ripples, which are harmful to long-term operation.

The electromagnetic torque expression of BDFM is obtained based on field energy theory:

$$T_{ep} = \frac{1}{2} p_p (i_r^T \frac{\partial L_{rp}}{\partial \theta_{rp}} i_p + i_p^T \frac{\partial L_{pr}}{\partial \theta_{rp}} i_r)$$

$$T_{ec} = \frac{1}{2} p_c (i_r^T \frac{\partial L_{rc}}{\partial \theta_{rc}} i_c + i_c^T \frac{\partial L_{cr}}{\partial \theta_{rc}} i_r) \qquad (8)$$

where L_{rp}, L_{pr}, L_{rc} and L_{cr} are the transient inductance matrices among the PW, rotor and CW. i_p, i_r and i_c are the transient current matrices of the PW, rotor and CW, respectively. T_{ep} and T_{ec} represent the torque generated by the magnetic field with two different pole pairs. The superscript "T" is the transpose of a matrix.

Through rotation transformation, the machine torque can be simplified to the current vector:

$$T_e = T_{ep} + T_{ec} = 1.5 p_p M_{pr} \text{Im}[i_p \hat{i}_r] - 1.5 p_c M_{cr} \text{Im}[i_c \hat{i}_r] \qquad (9)$$

where Im represents the imaginary part of complex-vector.

Furthermore, the unmeasurable rotor currents need to be replaced by i_p and i_c. Based on the rotor side in (5), by ignoring the small effects of R_r for the BDFM high slip characteristics, the relation among i_c, i_p and i_r can be expressed as:

$$-L_{sr} i_r = M_{pr} i_p + M_{cr} i_c. \qquad (10)$$

The right side of (10) represents the induced potential generated by two stator magnetic fields, which is balanced with the induced potential generated by the rotor magnetic field. Substituting (10) into (9), the relation among T_e, i_p and i_c is presented as:

$$T_e = 1.5 k_e \text{Im}[\hat{i}_p i_c] \qquad (11)$$

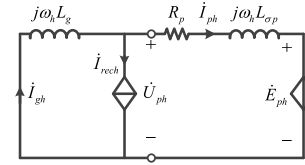where $k_e = (p_p + p_c) M_{pr} M_{cr} / L_{sr}$

FIGURE 4. The harmonic equivalent circuit considering BDFM as a voltage source.

According to (7), the detailed torque equation can be identified:

$$\begin{cases} T_{e0} = 1.5 k_e \text{Im}[\hat{i}_p^1 i_c^1 + \hat{i}_p^5 i_c^7 + \hat{i}_p^7 i_c^5] \\ T_{e6} = 1.5 k_e \text{Im}[(\hat{i}_p^1 i_c^5 + \hat{i}_p^5 i_c^1) e^{-j6\omega_p t} + (\hat{i}_p^7 i_c^1 + \hat{i}_p^1 i_c^7) e^{j6\omega_p t}] \\ T_{e12} = 1.5 k_e \text{Im}[\hat{i}_p^5 i_c^5 e^{-j12\omega_p t} + \hat{i}_p^7 i_c^7 e^{j12\omega_p t}]. \end{cases} \qquad (12)$$

It is easy to find that the torque includes 6th-order (T_{e6}) and 12th-order (T_{e12}) terms besides the DC component (T_{e0}). T_{e12} is generated by the interaction of harmonic components, which can be ignored for the small value. The major torque ripple component is T_{e6}, which contains fundamental and harmonic terms. It can be considered that T_{e6} is zero, and the setting value i_{ch}^* under this condition can be obtained. However, the calculated i_{ch}^* may have difficulty achieving the control target (eliminating T_{e6}) for the small value of i_{ph} and the error of machine parameters.

According to (12), if i_{ph} and i_{ch} are weakened at the same time, T_{e6} and T_{e12} would be effectively suppressed. Combining PW flux linkage equations in (5) and (10), the relation among i_p, i_c and Ψ_p can be obtained:

$$\frac{M_{pr} M_{cr}}{L_{sr}} i_c = \frac{L_{sp} L_{sr} - M_{pr}^2}{L_{sr}} i_p - \psi_p \qquad (13)$$

It can be seen from (13) that i_c can change along with i_p. When i_{ph} is reduced, i_{ch} will also decrease. Therefore, suppressing the torque ripple T_{e6} can be equivalent to eliminating the 5th negative sequence and 7th positive sequence harmonic contents in i_p. In other words, the equivalent harmonic impedance of the machine is increased and the effect of the harmonic current source i_{rech} on the machine is weakened. Controlling the PW harmonic currents to zero can be defined as the control target I. It can be expressed as:

$$i_{ph} = 0. \qquad (14)$$

B. THE HARMONIC CURRENT INJECTED INTO THE GRID

It can be seen in Fig. 2(b), the harmonic currents flowing into the grid will produce a corresponding voltage dip on L_g, which can indirectly affect $\dot{U}_{ph}$. Assuming the BDFM as a voltage source, the equivalent voltage $\dot{E}_p$ in the system circuit is shown in Fig. 4.

From the circuit in Fig. 4, it can be seen that the current $\dot{I}_{gh}$ can be divided into two parts, $\dot{I}_{gh1}$ and $\dot{I}_{gh2}$, generated by $\dot{I}_{rech}$ and $\dot{E}_{ph}$, respectively. Thus, $\dot{I}_{gh}$ can be controlled by regulating $\dot{E}_{ph}$. Based on superposition theory, the currents

Z. Li et al.: Bidirectional Harmonic Current Control of BDFM Drive System Based on a Fractional Unidirectional Converter

IEEE Access

$\dot{I}_{gh1}$ and $\dot{I}_{gh2}$ can be derived as:

$$\begin{cases} \dot{I}_{gh1} = \dot{I}_{rech}\dfrac{R_p + j\omega_h L_{\sigma p}}{j\omega_h L_g + R_p + j\omega_h L_{\sigma p}} \\ \dot{I}_{gh2} = -\dot{E}_{ph}\dfrac{1}{j\omega_h L_g + R_p + j\omega_h L_{\sigma p}}. \end{cases} \quad (15)$$

To eliminate the harmonic currents injected into the grid, the currents $\dot{I}_{gh1}$ and $\dot{I}_{gh2}$ should satisfy (16)

$$\dot{I}_{gh} = \dot{I}_{gh1} + \dot{I}_{gh2} = 0. \quad (16)$$

Combining (15) and (16), the value of $\dot{E}_{ph}$ can be obtained as:

$$\dot{E}_{ph} = \dot{I}_{rech}(R_p + j\omega_h L_{\sigma p}). \quad (17)$$

In the BDFM control system, the parameters that can be measured directly are $\dot{U}_{ph}$ and $\dot{I}_{ph}$. According to the grid side equivalent circuit shown in Fig. 4, the relation among $\dot{U}_{ph}$, $\dot{I}_{ph}$, $\dot{I}_{rech}$ and $\dot{E}_{ph}$ can be expressed as:

$$\begin{cases} \dot{I}_{ph} = \dfrac{\dot{U}_{ph} - \dot{E}_{ph}}{R_p + j\omega_h L_{\sigma p}}, \\ \dot{U}_{ph} = \dfrac{j\omega_h L_g \dot{E}_{ph}}{R_p + j\omega_h (L_g + L_{\sigma p})} - \dfrac{j\omega_h L_g (R_p + j\omega_h L_{\sigma p})\dot{I}_{rech}}{R_p + j\omega_h (L_g + L_{\sigma p})} \end{cases} \quad (18)$$

where $\dot{E}_{ph}$ and $\dot{I}_{rech}$ represent the effects of the control system and rectifier bridge, respectively.

By substituting (17) into (18), the control targets of $\dot{U}_{ph}$ and $\dot{I}_{ph}$ can be derived as:

$$\dot{U}_{ph} = 0 \quad \dot{I}_{ph} = -\dot{I}_{rech}. \quad (19)$$

In (19), the value of $\dot{U}_{ph}$ shows the nature of harmonic currents compensating from the circuit view, which makes the machine equivalent harmonic impedance small enough. Thus all harmonic currents will flow into the machine. $\dot{U}_{ph}$ is selected as the control parameter to avoid the measurement of $\dot{I}_{gh}$. The elimination of the harmonic currents injecting into the weak grid can be defined as the control target II. The detailed constraint conditions are further expressed as:

$$u_{p5}^5 = 0 \quad u_{p7}^7 = 0 \quad (20)$$

where the superscripts "5" and "7" denote the synchronously rotating reference frames of the 5th and 7th harmonic components, respectively.

C. TRADITIONAL PI CONTROL METHOD PERFORMANCE

Generally, the vector control system is built in the grid synchronously rotating reference frame. This section analyses the performance of the traditional control method in a weak grid.

Based on the CW equation of voltage and flux in (5), the relation among u_c, i_c, and i_r can be obtained as:

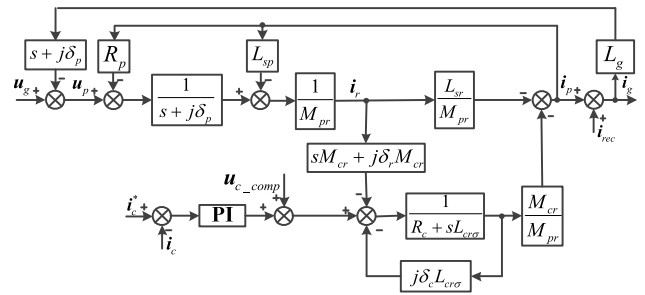$$u_c = (R_c + sL_{sc})i_c + j\delta_c L_{sc}i_c + (sM_{cr} + j\delta_c M_{cr})i_r. \quad (21)$$

FIGURE 5. The system transfer function structural diagram of conventional method.

Substituting (10) into (21), the unmeasurable rotor currents can be replaced by i_p and i_c, and the CW voltage equation can be rewritten as:

$$u_c = \underbrace{(R_c + sL_{cr\sigma})i_c}_{\text{direct part}} + \underbrace{j\delta_c L_{cr\sigma}i_c - (s + j\delta_c)\frac{M_{cr}M_{pr}}{L_{sr}}i_p}_{\text{coupling part}} \quad (22)$$

where $L_{cr\sigma} = L_{sc} - (M_{cr}^2/L_{sr})$

It can be seen that the inner loops can be established based on (22). The part directly related to i_c can be designed as a PI controller, and the coupling terms u_{c_comp} will be compensated to the output u_c^*:

$$u_c^* = (k_p + k_i/s)(i_c^* - i_c) + u_{c\_comp}. \quad (23)$$

Thus, the structure of the current control loop and machine model is shown in Fig. 5. It can be seen that the system contains three input sources, i.e., i_c^*, u_g, and i_{rec}. u_g represents the ideal grid which is the basic power of the system. i_{rec} is the nonlinear load injecting harmonic currents into the system. i_c^* represents the control loop effects on the system.

According to the system structure diagram shown in Fig. 5, the transfer functions of i_p and i_g can be obtained:

$$\begin{cases} i_p = G_{1irecPI}i_{rec} + G_{1ugPI}u_g + G_{1icPI}i_c^* \\ i_g = G_{2irecPI}i_{rec} + G_{2ugPI}u_g + G_{2icPI}i_c^* \end{cases} \quad (24)$$

where the detailed expressions of G_{1ugPI}, $G_{1irecPI}$, G_{1icPI}, G_{2ugPI}, $G_{2irecPI}$ and G_{2icPI} are shown in the appendix.

$G_{1irecPI}$ and $G_{2irecPI}$ in (24) represent the influence of the source i_{rec} on i_p and i_g under the conventional control structure. The prototype parameters and grid impedance provided in section II are used to study the system response characteristics. The rotor speed is set to 1200 rpm. Then, the Bode diagrams of $G_{1irecPI}$ and $G_{2irecPI}$ are shown in Fig. 6(a) and (b), respectively.

The increasing cut-off frequency of the PI controller has almost no effect on the damping of the harmonic source at 300 Hz. The magnitude frequency response data −1.37 dB and −16.7 dB in Fig. 6 represent the harmonic current distribution in different branches shown in Fig. 2(b), which is determined by the system parameters. The magnitude frequency response of $G_{1irecPI}$ and $G_{2irecPI}$ at 300 Hz represented regulating ability on the equivalent harmonic impedance of the machine system. Obviously, it is difficult to
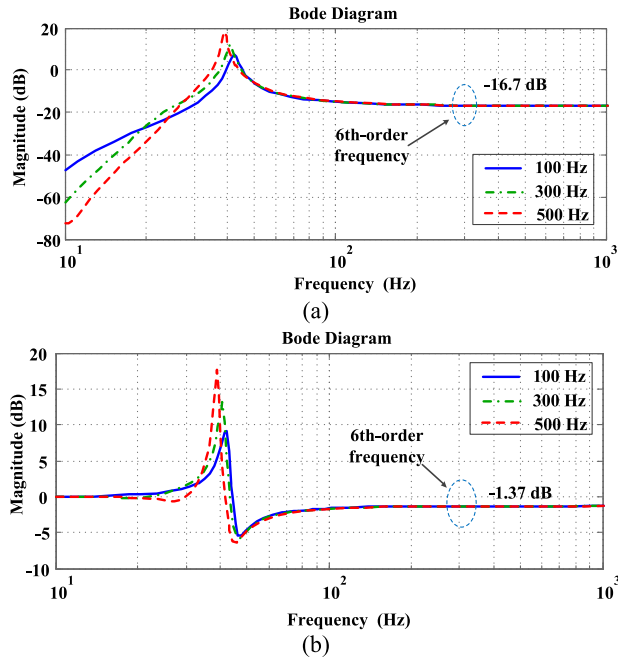
FIGURE 6. PW currents and the grid current sensitivity to the diode rectifier current in conventional control structure: (a) Magnitude frequency response of $G_{1irecPI}$; (b) Magnitude frequency response of $G_{2irecPI}$.

regulate the equivalent harmonic impedance by changing the bandwidth of the inner loops under the conventional mode. Thus, the control system structure needs to be optimized.

IV. OPTIMIZATION AND ANALYSIS OF THE CONTROL SYSTEM

A. CONTROL STRUCTURE OPTIMIZATION

The two control target settings in this paper are shown in (14) and (20). According to (7), the negative sequence 5th-order and positive sequence 7th-order components in i_p and u_p are shown as 6th-order harmonics in the fundamental synchronous rotating coordinate system, which will not be changed by the system operating state. Compared with the PI control under the 5th-order and 7th-order synchronous rotating coordinate system, the resonant controller has advantages in terms of dynamic response and saving calculation time for the coordinate transform. The transfer function of the 6th frequency resonance controller is shown as:

$$G_R = k_r \frac{2\omega_R s}{s^2 + 2\omega_R s + 36\omega_p^2} \qquad (25)$$

where k_r is the gain of the resonant controller and ω_R is the cut-off frequency that provides proper resonant bandwidth.

As shown in Fig. 5, i_p and u_p are related to u_c. On the basis of (22), the new u_c^* can be obtained as:

$$u_c^* = (k_p + k_i/s)(i_c^* - i_c) + u_{c\_comp} - u_{c\_R} \qquad (26)$$

where u_{c_R} represents the output of the resonance control loop under target I and target II.

According to (26) and the previous analysis, a new control structure can be given in Fig. 7. The "**R**" shown in Fig. 7
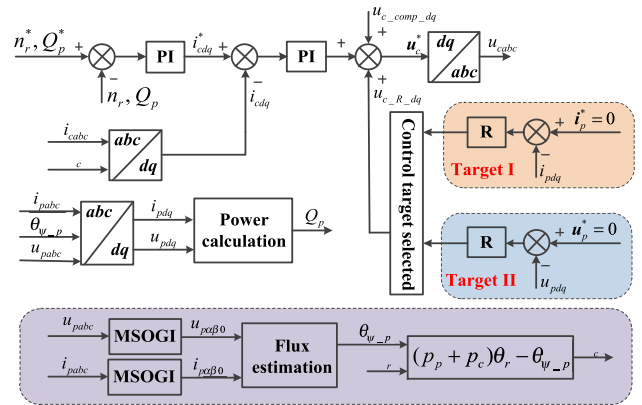
represents the resonant controller. Its detailed transfer function is presented in (25).

The PW flux orientation control method is applied in the following experiment. Generally, PW flux vector can be obtained through the integration of the induced potential:

$$\psi_{p\alpha\beta} = \int (u_{p\alpha\beta} - R_p i_{p\alpha\beta}) dt. \qquad (27)$$

The 5th and 7th harmonic components in $u_{p\alpha\beta}$ and $i_{p\alpha\beta}$ will produce disturbances in the calculation of the flux vector angle. In Fig. 7, the MOSGI-FLL method in [21] is introduced to obtain the accurate fundamental values of $u_{p\alpha\beta}$ and $i_{p\alpha\beta}$. It is based on a harmonic decoupling method making up of multiple second-order generalized integrators (MSOGIs) for calculating the different harmonic components in the distorted waveform and a frequency-locked loop (FLL) for estimating the fundamental frequency of the PW. Then, the angle of $\mathbf{\Psi}_p$ can be obtained for the fundamental reference frame.

Under a weak grid, the PCC voltage will obviously change along with the load power because of the impedance voltage drop. The THD of PCC voltage will increase with the increasing output power of the converter. Fundamental components of PW voltages and currents should be calculated accurately when the load changed suddenly. Then, the angle of the PW flux vector can be well tracked and the system stability would be maintained. Fig. 8 gives the simulation results of MOSGI-FLL while an 11 kW diode rectifier load switched in the weak grid shown in Fig. 1 suddenly.

From top to bottom of Fig. 8, the waveforms are the phase voltages of PCC, the calculating phase angle of the fundamental voltage vector and the calculating $\alpha\beta$ values of the fundamental voltages. It can be seen that the performance of MOSGI-FLL can meet the controller requirement and the influence of grid impendence on the system stability can be eliminated.

B. ANALYSIS OF THE NEW CONTROL METHOD

The two control loops corresponding to target I and target II do not operate at the same time. One of them will be selected as the resonance controller output according to the system
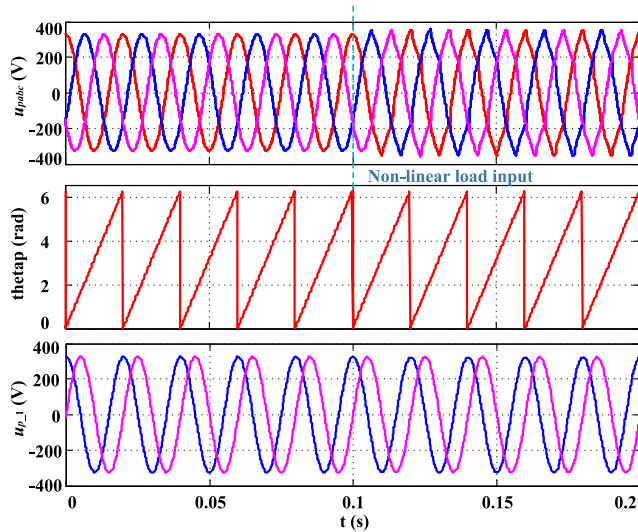

FIGURE 7. The proposed harmonic current control structure for a BDFM system with fractional unidirectional converter in a weak grid.

Z. Li et al.: Bidirectional Harmonic Current Control of BDFM Drive System Based on a Fractional Unidirectional Converter

IEEE Access·

FIGURE 8. Simulation results of the MSOGI-FLL with an 11 kW diode rectifier load switched in the weak grid.
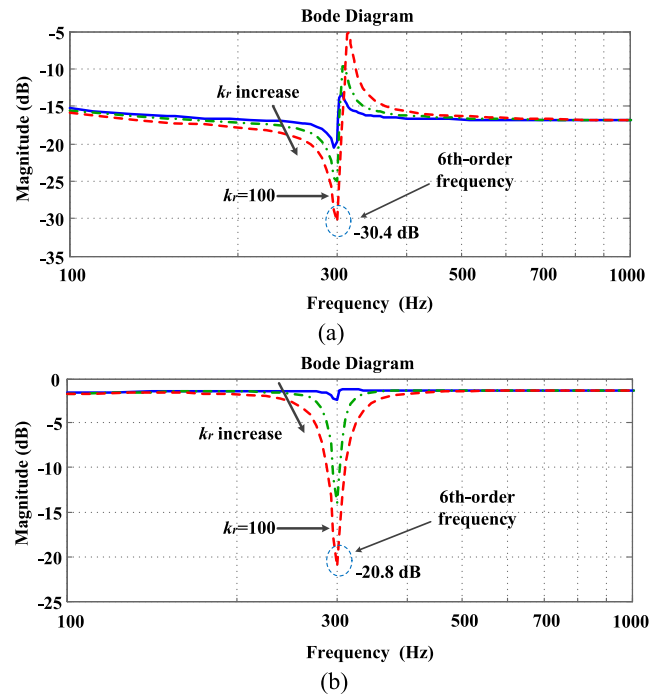

FIGURE 9. PW currents and the grid current sensitivity to the diode rectifier current in proposed control structure: (a) Magnitude frequency response of $G_{1irecPIR}$; (b) Magnitude frequency response of $G_{2irecPIR}$.

requirement. Based on Fig. 7 and Fig. 5, i_{gh} and i_{ph} depend on i_{rech} and two resonance control loops.

In the new control structure, (24) can be rewritten as:

$$\begin{cases} i_p = G_{1irecPIR}i_{rec} + G_{1ugPIR}u_g + G_{1icPIR}i_c^* \\ i_g = G_{2irecPIR}i_{rec} + G_{2ugPIR}u_g + G_{2icPIR}i_c^* \end{cases} \quad (28)$$

where the detailed expressions of G_{1ugPIR}, $G_{1irecPIR}$, G_{1icPIR}, G_{2ugPIR}, $G_{2irecPIR}$, and G_{2icPIR} are shown in the appendix.

An sufficient gain can be maintained within a certain range of the resonance point frequency for the ω_R. The greater gain of the resonant controller at the resonance point would be obtained with a smaller ω_R. However, the gain of the resonant controller will decay rapidly when the frequency deviates from the resonance point. The resonance point of the controller designed in this paper is fixed at 300 Hz. If the grid frequency fluctuates, the deviation of its 6th frequency relative to 300 Hz will be amplified 6 times. In order to ensure the performance of the resonance controller, ω_R is set to 18.8 rad/s, and the corresponding bandwidth frequency is 3 Hz. The cut-off frequency of the inner PI controller is set to 100 Hz. Then, the magnitude frequency response curves shown in Fig. 9 are obtained. Fig. 9(a) and (b) are corresponding to $G_{1irecPIR}$ and $G_{2irecPIR}$, respectively. The system parameters and operating state are similar to those in Fig. 6. Fig. 9 shows that the gain of i_{rec} relative to i_p or i_g is significantly reduced at the 6th-order frequency after the resonance control loop is added, and the decreased value increases with the increasing k_r. In addition, the equivalent harmonic impedance of machine system is changed with the control targets. Therefore, the two control targets can be realized through the new resonance controllers.

A resonant peak appears nearby the resonant frequency in Fig. 9(a), which also increases with the increasing k_r. In this case, the value of k_r should not be too large for the system steady operation.
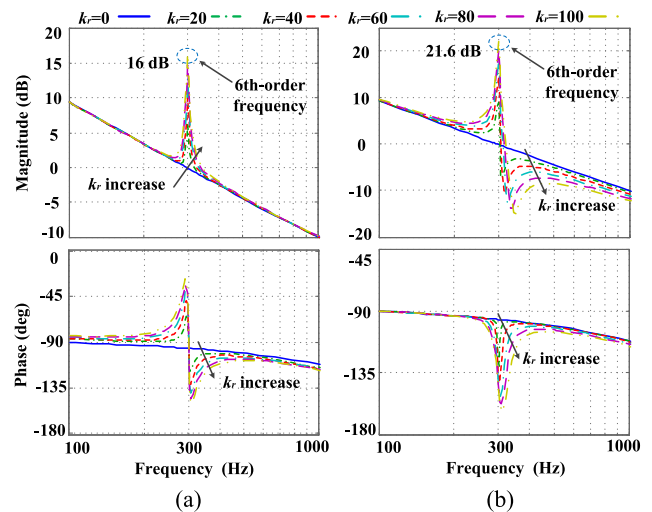
FIGURE 10. Bode diagrams of the open-loop transfer function in (28) with different k_r: (a) target I; (b) target II.

In order to analyze the impact of k_r on system stability, the bode diagrams of the open-loop transfer functions shown in (28) with different values of k_r are presented in Fig. 10.

It can be seen that a sudden change appears in the phase-frequency characteristic curves near the resonance point. The system phase margin is reduced after the application of resonant controller. A small phase margin will cause system oscillation. However, a large k_r can enhance the harmonic control ability. Considering the system stability and the controller gain comprehensively, k_r is selected as 40 and 50 under the control target I and II, respectively.

IEEE Access

Z. Li *et al.*: Bidirectional Harmonic Current Control of BDFM Drive System Based on a Fractional Unidirectional Converter

C. THE ALLOWANCE OF DC BUS VOLTAGE

In the conventional control mode, the current inner regulator output $\boldsymbol{u}_{cdq}^*$ presents as a DC component. After the resonance controllers are applied, a 6th-order frequency AC component is superimposed on the original output. To demonstrate the resonance controller effects on the $\boldsymbol{u}_c^*$ amplitude, the expression of $\boldsymbol{u}_c^*$ should be derived.

Substituting (14) into (5), the required $\boldsymbol{u}_c^*$ to realize target I can be given as:

$$\boldsymbol{u}_{c\_I} \approx \frac{\delta_c}{\delta_p} k_1 \boldsymbol{u}_{p0}^0 + [1 + \frac{(p_p + p_c)\omega_r}{5\omega_p}] k_1 \boldsymbol{u}_{p5}^5 e^{j6\omega_p t}$$
$$+ [1 - \frac{(p_p + p_c)\omega_r}{7\omega_p}] k_1 \boldsymbol{u}_{p7}^7 e^{-j6\omega_p t}. \quad (29)$$

Similarly, by substituting (19) into (5), the required $\boldsymbol{u}_c^*$ to realize target II can be derived as:

$$\boldsymbol{u}_{c\_II} \approx \frac{\delta_c}{\delta_p} k_1 \boldsymbol{u}_{p0}^0 + j[5\omega_p + (p_p + p_c)\omega_r] k_2 \boldsymbol{i}_{p5}^5 e^{j6\omega_p t}$$
$$- [7\omega_p - (p_p + p_c)\omega_r] k_2 \boldsymbol{i}_{p7}^7 e^{-j6\omega_p t} \quad (30)$$

where k_1 and k_2 are presented as:

$$\begin{cases} k_1 = (M_{cr}^2 - L_{sr}L_{sc})/M_{cr}M_{pr} \\ k_2 = (L_{sp}L_{sr}L_{sc} - L_{sc}M_{pr}^2 - L_{sp}M_{cr}^2)/M_{cr}M_{pr}. \end{cases}$$

Ignoring the system loss, according to (1) and (2), the relation between the converter output power and the machine speed is expressed as:

$$P_c \approx T_e(\omega_r - 60\frac{\omega_p}{p_p + p_c}). \quad (31)$$

Assuming the machine speed is constant, P_c will reach the maximum value under the rated load torque. Meanwhile, the harmonic current amplitude of $\boldsymbol{i}_{rec}$ is the largest. Accurate $\boldsymbol{i}_{rec}$ data can be calculated through the method introduced in [22] when the system operates at different speeds under the rated load torque. Then, according to (29) and (30), the maximum amplitude of $\boldsymbol{u}_c$ can be obtained under the two control targets. As shown in Fig. 1, the DC bus voltage of the converter is established through the non-controlled rectifier. It can be considered that the bus voltage is approximately equal to the grid voltage amplitude. The relation between the maximum voltage amplitude of $\boldsymbol{u}_c$ and the bus voltage corresponding to the two control targets at different speeds is shown in Fig. 11.

The modulation ratio can reach 1.125 in the space vector modulation mode. It can be seen that the DC bus voltage is large enough to meet the requirement of target I. However, the increasing amplitude of $\boldsymbol{u}_c^*$ is too large to satisfy at high speed when selecting target II. Thus, the regulation ability of rejecting the harmonic currents flowing into the grid is limited. A constraint for the output of the resonance loop should be set.
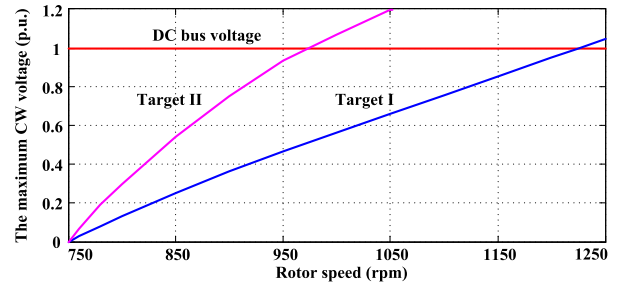

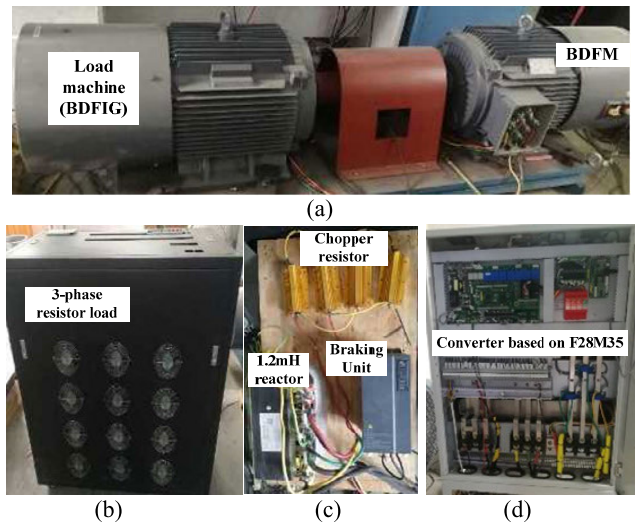**FIGURE 11.** The maximum CW voltages of the two control targets at different speeds.

FIGURE 12. The experimental platform of the BDFM system.

V. EXPERIMENTAL RESULTS

A. EXPERIMENTAL PLATFORM

The proposed harmonic current control method is verified on a 30 kW wound rotor BDFM experimental platform, as shown in Fig. 12.

A same power level brushless doubly fed generator shown in Fig. 12(a) is selected as the load, which is controlled through a back-to-back converter. The load PW connects to the three-phase resistive load directly, shown in Fig. 12(b). A 1.2 mH reactor shown in Fig. 12(c) is connected in series between the power grid and the unidirectional converter to simulate the power grid impedance. The converter shown in Fig. 12(d) is based on DSP F28M35, and the switching frequency is 3.125 kHz. The voltage and current sensors for the PW voltages, PW currents and CW currents are LV25-P(LEM), ALH-0.66(SIEMENS) and LT-308-S7/SP12(LEM), respectively. The rotor speed and position are obtained through an incremental encoder (E6B2-CWZ6C, OMRON). Experimental waveforms are collected based on a digital scope (DL850E, YOKOGAWA). The current inner loop PI parameters are set to $k_p = 2$ and $k_i = 40$. The parameters of the prototype are shown in Table 1, and the system topological structure is shown in Fig.1.
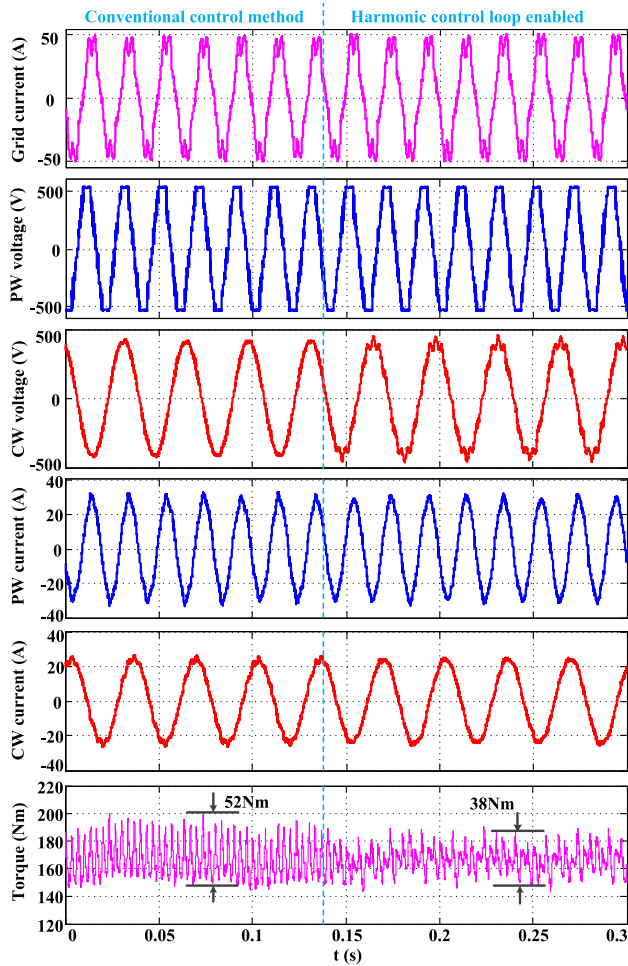
Z. Li *et al.*: Bidirectional Harmonic Current Control of BDFM Drive System Based on a Fractional Unidirectional Converter

IEEE *Access*

FIGURE 13. The transient performance under 21kW load condition when the resonance loop corresponding to target I is enabled.

TABLE 3. The harmonic data of two control methods corresponding to Fig. 13.

Harmonic order	Traditional method		Proposed method	
	I	II	I	II
i_{pa}(%)	4.40	1.91	1.65	0.73
i_{ca}(%)	3.80	1.53	1.46	0.56
u_{pab}(%)	4.04	2.91	4.33	2.99
i_{ga}(%)	14.29	7.10	14.86	7.33

Table 3 shows the harmonic contents in i_{pa}, i_{ca} and u_{pab} before and after the resonance controller is added. For i_{pa} and u_{pab}, I and II correspond to the 5th and 7th harmonics, respectively. For i_{ca}, they are the harmonics coupled with the 5th and 7th harmonics in i_{pa}, and the frequency relations are shown in Table 2. The 5th and 7th harmonic currents of i_{pa} decrease from 4.40% and 1.91% to 1.65% and 0.73% respectively by using the proposed controller.

According to the previous analysis, the equivalent harmonic impedance Z_M increases while the reduced harmonic content of i_p flows into the grid. Thus, the harmonic voltage drop on L_g is increased. The 5th and 7th harmonic voltages of u_{pab} rise from 4.04% and 2.91% to 4.33% and 2.99%, respectively. Compared with the initial values, the changed values are too small that the PW voltage waveform shown in Fig. 13 does not change obviously after the harmonic control loop being enabled.

The variation of machine electromagnetic torque during the switching of the control method is shown in the bottom of Fig. 13. According to (12), there is a positive correlation between the torque ripple and the harmonic of i_p. The amplitude of the torque ripple is reduced from 52 Nm to 38 Nm with the proposed control method.

Fig. 14 shows the dynamic performance of the system during speed variation. From the top to bottom, the waveforms are the PW current i_{pa}, the CW current i_{ca}, the rotor speed n_r and the CW voltage u_{cab} respectively. The speed is controlled linearly from 900 rpm to 1200 rpm in 6s while the load torque is 170 Nm. Control target I is selected, and the resonance controller is always enabled. The rotation speed changes smoothly, and the system operates stably throughout the process. The amplitude of the CW voltage increases with the raising of the CW frequency.

C. CONTROL TARGET II
Fig. 15 shows the system waveforms when selecting control target II (eliminating the harmonic currents injecting into the weak grid). From the top to bottom of Fig. 15, the waveforms are the grid current i_{ga}, the CW voltage u_{cab}, the PW current i_{pa} and the CW current i_{ca} respectively. At the initial stage, the conventional control method is applied, and the machine operates at 1000 rpm and 5 kW. The set value of Q_p^* is 4.77 kvar. The resonance controllers are enabled in 0.085s. k_r is set to 50, which rises to the set value linearly in 10 ms avoiding shock.

It's obvious that the harmonic content in i_{ga} is decreased and the waveform tends to sinusoidal after the resonance

B. CONTROL TARGET I
Fig. 13 presents the system response waveforms when selecting the control target I (controlling the PW harmonic currents to zero). From the top to bottom of Fig. 13, the waveforms are the grid current i_{ga}, the PW voltage u_{pab}, the CW voltage u_{cab}, the PW current i_{pa}, the CW current i_{ca} and the electromagnetic torque respectively. The converter works in traditional control mode under 1200 rpm, 21 kW before 0.14 s. The reactive power of the PW side is set to 4.77 kvar. In 0.14 s, the resonance control loop is enabled, and the controller parameter k_r is set to 40. To avoid shock, k_r rises to the set value linearly in 10 ms. It is clear that the grid current and PCC voltage are significantly distorted when the system operates under load on a weak grid. The waveform of u_{cab} is processed with a second-order low-pass filter (cut-off frequency is 1 kHz). After the resonance controller output is added, a smaller 300 Hz harmonic component is superimposed on u_{cab}. Its value increases with increasing k_r, and finally stabilizes. It can be seen that the harmonic content in i_{pa} is significantly reduced under the proposed method, which is consistent with the set control target. In addition, due to the correlation between i_{pa} and i_{ca}, the harmonic of i_{ca} is also suppressed.

IEEE *Access*

Z. Li *et al.*: Bidirectional Harmonic Current Control of BDFM Drive System Based on a Fractional Unidirectional Converter
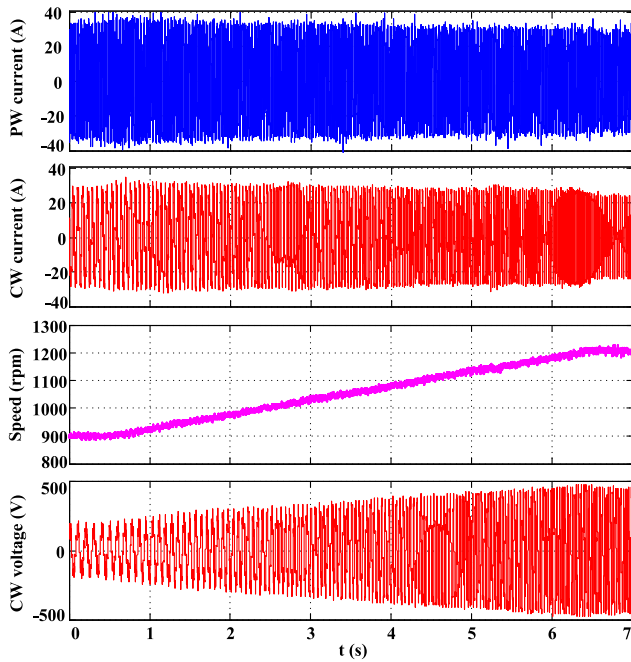

FIGURE 14. The performance of speed regulation process with 170 Nm load torque under the proposed method when selecting target I.
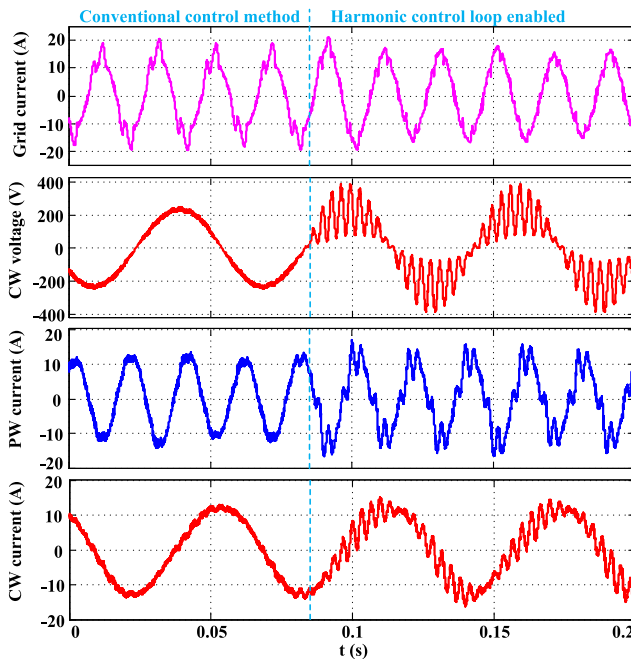

FIGURE 15. The transient performance when the resonance loop corresponding to target II is enabled.

regulator is enabled. Fig. 13 and Fig. 15 also show that the proposed method can be used for bidirectional harmonic currents control without additional devices. The harmonic currents generated by the diode rectifier can be controlled to flow into the weak grid or the machine system according to actual requirements. The waveform of converter output voltage is dealt with a second-order low-pass filtering (cut-off frequency is 1 kHz). The amplitude of u_{cab} is approximately

TABLE 4. The harmonic data of two control methods corresponding to Fig. 15.

	Traditional method		Proposed method	
Harmonic order	5th	7th	5th	7th
i_{ga}(%)	13.41	11.38	3.47	2.46
u_{pab}(%)	1.45	1.16	0.50	0.38
i_{pa}(%)	4.12	2.16	20.72	19.06

237 V before the resonance controller is enabled. When switching to the proposed control method, a larger 300 Hz harmonic component is superimposed on the original basis. There is no limitation on the output of the resonance control loop. The maximum value of u_{cab} reaches 400 V.

The waveform of PW current i_{pa} is clearly distorted after the control method switched. According to the equivalent circuit shown in Fig. 2(a), the machine harmonic equivalent impedance Z_m is reduced, and some parts of the harmonic currents existing in the grid are moved to the machine. From this perspective, the amplitude of the 6 times frequency torque ripple will be improved. Considering the limitation of DC bus voltage, the resonance regulator should be restricted based on the machine speed and load. According to the waveform of CW current shown in Fig. 15, its harmonic contents increase obviously due to the relation of i_p and i_c.

Table 4 gives the specific 5th- and 7th-order harmonic data of i_{ga}, u_{pab} and i_{pa} before and after the harmonic control loop is enabled.

It can be seen from the Table 4 that the 5th-order harmonic of u_{pa} is reduced from 1.45% to 0.5%, and the 7th-order harmonic of u_{pab} is decreased from 1.16% to 0.38%. The variation of the PW voltage harmonic components is small for the large value of fundamental component. Besides, the PW voltage harmonic components are only selected as the substitution parameters of grid currents harmonic components. Corresponding to the PW voltage, the 5th-order harmonic of i_{ga} is reduced from 13.41% to 3.47%, and the 7th-order harmonic of i_{ga} is decreased from 11.38% to 2.46%. The distribution of harmonic current in the weak grid and machine is changed by the proposed method. Thus, the control target II is well achieved.

Meanwhile, the 5th- and 7th-order harmonics of i_{pa} are increased from 4.12% and 2.16% to 20.72% and 19.06%, respectively. The higher harmonic current would increase the motor torque ripple and decrease the efficiency. In this view, a proper limitation on the regulation of grid harmonic currents is necessary.

VI. CONCLUSION

The BDFM variable speed drive system based on a fractional unidirectional converter has wide application prospects for loads that require only limited range speed regulation. To solve the influence of harmonics on system, this paper studies the harmonic characteristics through a new equivalent circuit and proposes a direct harmonic control strategy. It is shown that:

Z. Li *et al.*: Bidirectional Harmonic Current Control of BDFM Drive System Based on a Fractional Unidirectional Converter

IEEE *Access*

1) The harmonic current contents in the machine and the grid are determined by the grid harmonic impedance and the harmonic equivalent impedance of the machine system. Calculation results agree with the experiment data;

2) The nature of the bidirectional harmonic currents control between the weak grid and the machine is changing the harmonic distribution characteristics of the BDFM driving system shown in Fig. 1, while the conventional control method can hardly realize this target;

3) The torque ripples and the harmonic currents injecting into the grid can be controlled indirectly through i_{ph} and u_{ph};

4) The proposed control method can regulate the harmonic equivalent impedance of the machine system effectively, which commendably realizes the bidirectional harmonic current control.

The equivalent circuit structure and control method proposed in this paper are also suitable for distorted grid with a large number of nonlinear loads. In this operation environment, a single BDFM control system is insufficient to improve the grid, which will be studied in the future.

APPENDIX

The detailed expressions of coefficients in (24) and (28) are given in this appendix.

$$\begin{cases} G_{1irecPI} = \dfrac{-sL_g G_1}{(R_p + sL_g + L_{pr\sigma}G_p)G_1 - s^2L_M^2 G_p} \\ G_{1ugPI} = \dfrac{G_1}{(R_p + sL_g + L_{pr\sigma}G_p)G_1 - s^2L_M^2 G_p} \\ G_{1icPI} = \dfrac{sL_M G_p G_{PI}}{(R_p + sL_g + L_{pr\sigma}G_p)G_1 - s^2L_M^2 G_p}. \end{cases} \quad (32)$$

$$\begin{cases} G_{2irecPI} = \dfrac{(R_p + L_{pr\sigma}G_p)G_1 - s^2L_M^2 G_p}{(R_p + L_{pr\sigma}G_p + sL_g)G_1 - s^2L_M^2 G_p} \\ G_{2ugPI} = \dfrac{G_1}{(R_p + L_{pr\sigma}G_p + sL_g)G_1 - s^2L_M^2 G_p} \\ G_{2icPI} = \dfrac{sL_M G_p G_{PI}}{(R_p + L_{pr\sigma}G_p + sL_g)G_1 - s^2L_M^2 G_p}. \end{cases} \quad (33)$$

$$\begin{cases} G_{1irecPIR} = \dfrac{-sL_g G_1}{(R_p + sL_g + L_{pr\sigma}G_p)G_1 - (s^2L_M^2 + sG_R L_M)G_p} \\ G_{1ugPIR} = \dfrac{G_1}{(R_p + sL_g + L_{pr\sigma}G_p)G_1 - (s^2L_M^2 + sG_R L_M)G_p} \\ G_{1icPIR} = \dfrac{sL_M G_p G_{PI}}{(R_p + sL_g + L_{pr\sigma}G_p)G_1 - (s^2L_M^2 + sG_R L_M)G_p}. \end{cases} \quad (34)$$

$$\begin{cases} G_{2irecPIR} = \dfrac{(R_p + L_{pr\sigma}G_p)G_1 - s^2L_M^2 G_p}{(R_p + G_p L_{pr\sigma} + sL_g)G_1 - s^2(L_M^2 - G_R L_g L_M)G_p} \\ G_{2ugPIR} = \dfrac{G_1 + sL_M G_p G_R}{(R_p + G_p L_{pr\sigma} + sL_g)G_1 - s^2(L_M^2 - G_R L_g L_M)G_p} \\ G_{2icPIR} = \dfrac{sL_M G_p G_{PI}}{(R_p + G_p L_{pr\sigma} + sL_g)G_1 - s^2(L_M^2 - G_R L_g L_M)G_p}. \end{cases} \quad (35)$$

where the coefficients are presented as:

$$\begin{cases} L_{pr\sigma} = L_{sp} - M_{pr}^2/L_{sr} \\ L_M = M_{cr}M_{pr}/L_{sr}, \end{cases} \quad (36)$$

$$\begin{cases} G_{PI} = k_p + k_i/s \\ G_p = s + j\delta_p \\ G_1 = s^2 L_{cr\sigma} + sR_c + sG_{PI}, \end{cases} \quad (37)$$

REFERENCES

[1] X. Chen and X. Wang, "Proximate standing wave feature of magnetic field and its influence on the performance of wound rotor brushless doubly-fed machine," *IEEE Trans. Energy Convers.*, vol. 32, no. 1, pp. 296–308, Mar. 2017.

[2] J. Su, Y. Chen, D. Zhang, and Y. Kang, "Stand-alone brushless doubly fed generation control system with feedforward parameters identification," *IEEE Trans. Ind. Informat.*, vol. 15, no. 11, pp. 6011–6022, Nov. 2019.

[3] J. Chen, X. Wang, T. Zhao, Z. Li, M. Kong, and P. Nie, "Application of brushless doubly-fed machine system in hydropower generation," in *Proc. 22nd Int. Conf. Electr. Mach. Syst. (ICEMS)*, Harbin, China, Aug. 2019, pp. 1–4.

[4] T. D. Strous, H. Polinder, and J. A. Ferreira, "Brushless doubly-fed induction machines for wind turbines: Developments and research challenges," *IET Electr. Power Appl.*, vol. 11, no. 6, pp. 991–1000, Jul. 2017.

[5] M. Kong, X. Wang, Z. Li, and P. Nie, "Asynchronous operation characteristics and soft-starting method for the brushless doubly-fed motor," *IET Electr. Power Appl.*, vol. 11, no. 7, pp. 1276–1283, Aug. 2017.

[6] S. Shao, E. Abdi, and R. Mcmahon, "Low-cost variable speed drive based on a brushless doubly-fed motor and a fractional unidirectional converter," *IEEE Trans. Ind. Electron.*, vol. 59, no. 1, pp. 317–325, Jan. 2012.

[7] G. Zhang, J. Yang, Y. Sun, M. Su, W. Tang, Q. Zhu, and H. Wang, "A robust control scheme based on ISMC for the brushless doubly fed induction machine," *IEEE Trans. Power Electron.*, vol. 33, no. 4, pp. 3129–3140, Apr. 2018.

[8] J. Chen, W. Zhang, B. Chen, and Y. Ma, "Improved vector control of brushless doubly fed induction generator under unbalanced grid conditions for offshore wind power generation," *IEEE Trans. Energy Convers.*, vol. 31, no. 1, pp. 293–302, Mar. 2016.

[9] Y. Liu, W. Xu, J. Zhu, and F. Blaabjerg, "Sensorless control of standalone brushless doubly fed induction generator feeding unbalanced loads in a ship shaft power generation system," *IEEE Trans. Ind. Electron.*, vol. 66, no. 1, pp. 739–749, Jan. 2019.

[10] C. Liu, F. Blaabjerg, W. Chen, and D. Xu, "Stator current harmonic control with resonant controller for doubly fed induction generator," *IEEE Trans. Power Electron.*, vol. 27, no. 7, pp. 3207–3220, Jul. 2012.

[11] C. Wu and H. Nian, "Stator harmonic currents suppression for DFIG based on feed-forward regulator under distorted grid voltage," *IEEE Trans. Power Electron.*, vol. 33, no. 2, pp. 1211–1224, Feb. 2018.

[12] J. Hu, H. Xu, and Y. He, "Coordinated control of DFIG's RSC and GSC under generalized unbalanced and distorted grid voltage conditions," *IEEE Trans. Ind. Electron.*, vol. 60, no. 7, pp. 2808–2819, Jul. 2013.

[13] V.-T. Phan and H.-H. Lee, "Control strategy for harmonic elimination in stand-alone DFIG applications with nonlinear loads," *IEEE Trans. Power Electron.*, vol. 26, no. 9, pp. 2662–2675, Sep. 2011.

[14] Y. Liu, W. Xu, T. Long, and F. Blaabjerg, "An improved rotor speed observer for standalone brushless doubly-fed induction generator under unbalanced and nonlinear loads," *IEEE Trans. Power Electron.*, vol. 35, no. 1, pp. 775–788, Jan. 2020.

[15] *IEEE Recommended Practice and Requirements for Harmonic Control in Electric Power Systems*, IEEE Standard 519, 2014.

[16] R. A. McMahon, P. C. Roberts, X. Wang, and P. J. Tavner, "Performance of BDFM as generator and motor," *Proc. Inst. Elect. Eng.-Elect. Power Appl.*, vol. 153, no. 2, pp. 289–299, Mar. 2006.

[17] S. Williamson, A. C. Ferreira, and A. K. Wallace, "Generalised theory of the brushless doubly-fed machine. I. Analysis," *IEE Proc.-Electr. Power Appl.*, vol. 144, no. 2, pp. 111–122, Mar. 1997.

[18] P. C. Roberts, R. A. McMahon, P. J. Tavner, J. M. Maciejowski, and T. J. Flack, "Equivalent circuit for the brushless doubly fed machine (BDFM) including parameter estimation and experimental verification," *IEE Proc.-Electr. Power Appl.*, vol. 152, no. 4, pp. 933–942, Jul. 2005.

[19] P. Han, M. Cheng, X. Wei, and Y. Jiang, "Steady-state characteristics of the dual-stator brushless doubly fed induction generator," *IEEE Trans. Ind. Electron.*, vol. 65, no. 1, pp. 200–210, Jan. 2018.

[20] J. Poza, E. Oyarbide, D. Roye, and M. Rodriguez, "Unified reference frame dq model of the brushless doubly fed machine," *IEE Proc. Elect. Power Appl.*, vol. 153, no. 5, pp. 726–734, Sep. 2006.

IEEE *Access*

Z. Li *et al.*: Bidirectional Harmonic Current Control of BDFM Drive System Based on a Fractional Unidirectional Converter

[21] P. Rodriguez, A. Luna, I. Candela, R. Mujal, R. Teodorescu, and F. Blaabjerg, ''Multiresonant frequency-locked loop for grid synchronization of power converters under distorted grid conditions,'' *IEEE Trans. Ind. Electron.*, vol. 58, no. 1, pp. 127–138, Jan. 2011.

[22] M. Sakui, H. Fujita, and M. Shioya, ''A method for calculating harmonic currents of a three-phase bridge uncontrolled rectifier with DC filter,'' *IEEE Trans. Ind. Electron.*, vol. 36, no. 3, pp. 400–434, Aug. 1989.

ZHENPING LI received the B.S. degree in electrical engineering from Henan Polytechnic University, Jiaozuo, China, in 2013. He is currently pursuing the Ph.D. degree with the Department of Electrical and Control Engineering, School of Electrical and Electronic Engineering, Huazhong University of Science and Technology, Wuhan, China.

His research interests include modeling and control of brushless doubly fed induction machine.

XUEFAN WANG received the B.S., M.S., and Ph.D. degrees in electrical engineering from the Huazhong University of Science and Technology, Wuhan, China, in 1982, 1986, and 1989, respectively.

Since 2002, he has been a Professor with the State Key Laboratory of Advanced Electromagnetic Engineering and Technology, School of Electrical and Electronic Engineering, Huazhong University of Science and Technology. His current research interests include AC winding theory, magnetic field analysis, and design and control of electric machines.

MING KONG received the B.S. degree from the School of Energy and Power Engineering, Huazhong University of Science and Technology, Wuhan, China, in 2009, and the Ph.D. degree from the School of Electrical and Electronic Engineering, Huazhong University of Science and Technology, in 2018.

Since 2018, he has been working with EAST Group Company Ltd., Dongguan, China. His research interest includes control of electrical machine.
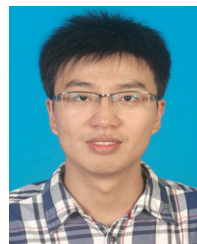
XI CHEN (Member, IEEE) was born in Zhengzhou, China. He received the B.Eng. degree from the Shenyang University of Technology, Shenyang, China, in 2012, and the Ph.D. degree from the Huazhong University of Science and Technology, Wuhan, China, in 2017, both in electrical engineering.

From 2017 to 2019, he was a Senior Research and Development Engineer with Envision Energy, Shanghai, China. In September 2019, he became a Postdoctoral Research Fellow with the State Key Laboratory of Advanced Electromagnetic Engineering and Technology, School of Electrical and Electronic engineering, Huazhong University of Science and Technology. His research interests include design and control of electrical machine systems, and renewable energy technologies.

• • •